Bioelectrochemistry 142 (2021) 107946

Contents lists available at ScienceDirect

Bioelectrochemistry

journal homepage: www.elsevier.com/locate/bioelechem

Adsorption of lysozyme on gold surfaces in the presence of an external electric potential

Paulina Komorek [a], Barbara Jachimska [a,*], Izabella Brand [b,*]

[a] Jerzy Haber Institute of Catalysis and Surface Chemistry Polish Academy of Sciences, Niezapominajek 8, 30-239 Cracow, Poland
[b] Department of Chemistry, University of Oldenburg, 26111 Oldenburg, Germany

ARTICLE INFO

Article history:
Received 27 May 2021
Received in revised form 30 July 2021
Accepted 29 August 2021
Available online 1 September 2021

Keywords:
Lysozyme adsorption
Gold surface
Secondary structure
Electric potential
Polarization modulation infrared reflection absorption spectroscopy

ABSTRACT

Adsorbed protein films consist of essential building blocks of many biotechnological and biomedical devices. The electrostatic potential may significantly modulate the protein behaviour on surfaces, affecting their structure and biological activity. In this study, lysozyme was used to investigate the effects of applied electric potentials on adsorption and the protein structure. The pH and the surface charge determine the amount and secondary structure of adsorbed lysozyme on a gold surface. In-situ measurements using polarization modulation infrared reflection absorption spectroscopy indicated that the concentration of both the adsorbed anions and the lysozyme led to conformational changes in the protein film, which was demonstrated by a greater amount of aggregated β-sheets in films fabricated at net positive charges of the Au electrode ($E_{ads} > E_{pzc}$). The changes in secondary structure involved two parallel processes. One comprised changes in the hydration/hydrogen-bond network at helices, leading to diverse helical structures: α-, 3_{10}- and/or π-helices. In the second process β-turns, β-sheets, and random coils displayed an ability to form aggregated β-sheet structures. The study illuminates the understanding of electrical potential-dependent changes involved in the protein misfolding process.

© 2021 The Authors. Published by Elsevier B.V. This is an open access article under the CC BY-NC-ND license (http://creativecommons.org/licenses/by-nc-nd/4.0/).

1. Introduction

The behaviour of protein systems on interfaces is determined by several factors. A significant part of the research conducted so far was focused on the analysis of the influence of the type of electrolyte and the nature of the adsorption surface in controlling the effects of the process of adsorption and its kinetics [1–5]. Electrostatic forces, arising from interactions between a solid surface and an adsorbing protein, determine the stability of the adsorbed film as well as the protein structure and conformation [6–12]. One exciting but considerably less understood factor influencing both the quantity of adsorbed molecules and the protein properties is the interfacial electric potential. It is of particular importance in materials science (designing of biosensors, drug delivery systems, and anti-fouling coatings), but plays a crucial role in natural systems as they produce and emit electric fields. Currently, many methods are used to monitor the macroscopic properties of protein layers, such as surface-enhanced resonance spectroscopy (SERS) [13], multi-parameter surface plasmon resonance (MP-SPR) [14], atomic force microscopy (AFM), quartz crystal microbalance (QCM-D), contact angle measurements (CA) [15], or simulations using molecular dynamics (MD) [10,16]. A feature of particular importance for the biomedical area is the activity and function of proteins directly related to their secondary structure [17–20]. It has been reported that native secondary structure elements of a protein may be strongly influenced by electrical fields [21,22], leading even to incorrect folding, aggregation, or to amyloid formation [23]. Such considerable changes in conformation can be associated with the development of many disorders, such as Alzheimer's disease, Parkinson's disease, encephalopathy, or type II diabetes [24–27]. To better understand the stability of the selected protein system, the influence of different surface-charge densities caused by the electrical potential should be examined in the context of the secondary and tertiary structure's internal stability. The effect of electrical potentials on the structure of proteins during adsorption was demonstrated by several computer-simulation studies [10–12,28–30]. However, there are very few experimental results providing useful information on the conformation of the protein under the conditions of varied surface charge densities. This dearth is due to the complexity of this type of experiment, mainly the limitations of many measurement techniques. Therefore, in the current work, in situ polarization modulation infrared reflection absorption spectroscopy (PM IRRAS) was used to obtain qualitative and quantitative data on the effect of electri-

* Corresponding authors.
E-mail addresses: barbara.jachimska@ikifp.edu.pl (B. Jachimska), izabella.brand@uol.de (I. Brand).

https://doi.org/10.1016/j.bioelechem.2021.107946
1567-5394/© 2021 The Authors. Published by Elsevier B.V.
This is an open access article under the CC BY-NC-ND license (http://creativecommons.org/licenses/by-nc-nd/4.0/).

cal potentials on the adsorption efficiency and conformation of adsorbed molecules. It has previously been reported that this technique is perfect for identifying changes in the structure of the synthetic polymers [31,32], and biopolymer films [33,34] under the influence of the applied potential in real-time measurements. Here, we explored the potential of PM IRRAS for the investigation of changes in the conformation of adsorbed protein under external electrical potentials. In our adsorption studies, lysozyme, which is characterized by high conformational stability, was used. Nevertheless, literature reports indicate that changes in the lysozyme structure may occur under extreme experimental conditions, leading even to amyloidogenic properties and the formation of amyloid precursors [35]. The influence of conformational changes in lysozyme towards aggregation and amyloidosis under the influence of internal factors, such as high temperature and various types of solvents [36–38] has been intensively investigated. In contrast, studies on factors such as the substrate electrical potential or surface charge density were rarely conducted [10]. Due to the fact that the process of changes in the secondary structure as a result of adsorption is not yet fully understood, we investigated the influence of the external electrical potentials and different charge densities at the solid surface on the conformation of the lysozyme in the adsorbed state.

2. Materials and methods

2.1. Materials

Lysozyme (L6876) was purchased from *Sigma-Aldrich* (Steinheim, Germany). The concentration of lysozyme was equal to 100 ppm in 0.01 M NaCl in H_2O (resistivity 18.2 MΩ cm, PureLab Classic, *Elga LabWater*, Celle, Germany) or in D_2O electrolyte solution (*Euroisotop*, Saarbrücken, Germany). The pH (pD) of the electrolyte solution was adjusted to 4.0, 7.5, and 9.0 by adding HCl (DCl) (*Sigma-Aldrich*, Steinheim, Germany) or NaOH (NaOD) (*Sigma Aldrich*, Steinheim, Germany). Before use, fresh samples were prepared. The measurements were carried out at room temperature (298 K).

2.2. Methods

2.2.1. Quartz microbalance with energy-dissipation monitoring (QCM-D)

The process of lysozyme adsorption was performed using a quartz crystal microbalance with energy-dissipation monitoring using Q-Sense E1 (*Biolin Scientific*, Espoo, Finland). The method allows determining the mass of molecules attached to the QCM-D sensor and the monitoring of energy dissipation. The value of dissipation gives information about the viscoelastic properties of films formed. Both of the parameters (the change in the resonance frequency Δf and the difference in the energy dissipation ΔD) were recorded during the measurements. As the changes in energy dissipation were low, the mass of lysozyme layers (Γ_{QCM-D}) was calculated based on the Sauerbrey equation:

$$\Gamma_{QCM-D} = -C\frac{\Delta f}{n} \quad (1)$$

where Δf is the change in the resonance frequency (Hz), C is a constant characteristic of quartz crystals and equal to 17.7 ng/cm^2 Hz, and n is the number of overtones. The model is appropriate for thin, homogenous, and rigid layers. According to Eq. (1), the change in the resonance frequency is proportional to the change in the QCM-D mass. As no considerable differences were noted for successive overtones in the system under examination, the results were presented only for the 7th overtone (n = 7).

2.2.2. Electrochemical measurements

Electrochemical measurements were performed in an all-glass, three-electrode cell using a polycrystalline Au disc (dia. 15 mm, *Alfaaeser*, Karlsruhe, Germany) as the working electrode (WE). A gold wire was used as a counter electrode (CE), and a Ag|AgCl| sat.KCl (Ag|AgCl) as a reference electrode (RE). The WE was immersed in the electrochemical cell in a hanging meniscus configuration. A *Methrom Autolab* potentiostat (Utrecht, Netherlands) was used to perform the electrochemical measurements. Before the experiment, the cell was purged with argon for 30 min. The electrochemical cell's cleanness was tested by recording potential capacitance plots of the polycrystalline Au electrode in 0.01 M NaCl in H_2O as a solvent, with pH adjusted with either HCl or NaOH to 4.0, 7.5, or 9.0. Alternative current voltammetry (ACV) was used to measure the capacitance of the unmodified and lysozyme modified polycrystalline Au electrode. AC voltammograms were recorded in negative- and positive-going potential scans at a rate 5 mV s^{-1} and the perturbation of the AC signal of 20 Hz and 10 mV amplitude. The differential capacitance versus potential curves were calculated from the in-phase and out-of-phase components of the AC signal assuming the cell was equivalent to a resistor in series with a capacitor (Fig. S1). An electrolyte solution containing 100 ppm of lysozyme was added to a clean electrochemical cell, which was then purged with Ar for 30 min. Chronocoulometry experiments were used to control the lysozyme's adsorption from the electrolyte solution onto the Au electrode surface. The potential step from the open circuit potential to a selected adsorption potential (E_{ads}) was realised, and the E_{ads} held constant for 90 min. The E_{ads} applied to the Au electrode corresponded to net negative (ca. −10 μC cm^{-2}) and positive (ca. 15 μC cm^{-2}) surface-charge densities of the unmodified Au electrode. The adsorption of lysozyme affected the surface charge density and potential of zero charge of the Au electrode. Since the capacitance curves did not clearly show desorption of the protein molecules from the gold surface, the zero total charge potential was not determined, but the applied potentials corresponded to similar charge densities of the unmodified Au electrode in solutions with different pH values. The E_{ads} depended on the pH of the electrolyte solution, and was equal to −0.25 V and 0.35 V for a solution with pH = 4; −0.3 V and 0.30 V for pH = 7.5; and −0.65 V and 0 V for pH = 9. To remove unspecifically adsorbed protein after the adsorption, the modified Au electrode was immersed for 90 min in the pure electrolyte solution with the corresponding pH value. Finally, the modified electrode was immersed into D_2O to remove associated Na^+ and Cl^- from the film. Additionally, to verify the influence of Cl^- on the process of lysozyme adsorption, analogous experiments were performed in 0.01 M NaF electrolyte solution (pH = 7.5) for conditions $E > E_{pzc}$. The selected E_{ads} equalled 0.30 V.

2.2.3. PM IRRAS measurements

The PM IRRA spectra were recorded using a Vertex 70 spectrometer with a photoelastic modulator (f = 50 kHz; PMA 50, *Bruker*, Ettingen, Germany) and demodulator (*Hinds Instruments*, OR, USA). A home-made spectroelectrochemical glass cell was washed in water, then in ethanol solution, and dried in an oven at 60 °C. After rinsing the CaF_2 prism with water and ethanol, it was cleaned using a UV ozone chamber (*Bioforce Nanosciences*, VA, USA) for 10 min. The spectroelectrochemical cell had a built-in platinum CE. The RE was Ag|AgCl in 3 M KCl in D_2O. A disc polycrystalline gold electrode (dia. 15 mm, *Alfaaeser*, Karlsruhe, Germany) was used as the WE and as a mirror for the IR radiation. The lysozyme film was adsorbed on the gold surface according to the procedure described above in Section 2.2. The electrolyte solution was 0.01 M NaCl in D_2O, with pD adjusted to 4.3, 7.5, or 9.3. The difference between pH and pD is ca. 0.3. The electrolyte solution was purged for 1 h with argon to remove oxygen. At each potential applied to

the Au electrode, 400 spectra with a resolution of 4 cm^{-1} were measured. To analyse the amide I mode in the protein, the half-wave retardation was set to 1600 cm^{-1}. The angle of incidence of the incoming IR radiation was 55°. The thickness of the electrolyte layer between the CaF_2 prism and Au electrode was 4.2 ± 0.5 μm. A potential cycle was composed of a negative- and positive potential scans. In each potential scan different potentials were applied to the Au electrode, depending on the pD of the electrolyte solution, as summarized in Table 1. In each experiment, 6 potential scans were measured. The spectra shown in this paper correspond to the average obtained from two independent measurements. The analysis of PM IRRA spectra was carried out using the OPUS v5.5 software (*Bruker*, Ettlingen, Germany). The qualitative and quantitative analysis of the secondary structure elements of lysozyme adsorbed on the gold electrode under the range of applied potentials was carried out after background correction and normalization of spectra.

3. Results and discussion

3.1. Physicochemical properties of lysozyme

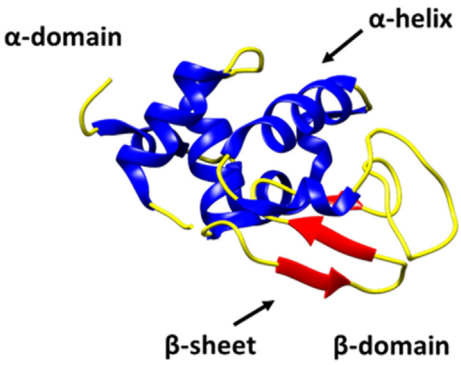
Lysozyme is considered to be an elliptical molecule, with dimensions of 45 Å × 30 Å × 30 Å [39,40]. Its isoelectric point is in pH = 10 and the charge across the protein surface is not spread equally [41]. Lysozyme consists of one polypeptide chain, 129 amino acids long and cross-linked by four disulfide bridges. The lysozyme molecule is built of two main parts: an α-domain composed of four helices corresponding to residues: 4–15, 24–36, 89–99 and 108–115; a β-domain consisting of three β-sheet structures (residues: 41–45, 50–53); a long loop (residues 61–78) and a short 3_{10}-helix (residues 80–84) [42]. The simplified structure of the lysozyme is presented in Scheme 1.

Lysozyme is regarded as a hard protein because its structure is stable and resistant to denaturation. In Fig. 1, measurements performed by circular dichroism (CD) in the UV–Vis wavelength spectral region (185–250 nm) for lysozyme in the pH range 3 to 10, 0.01 M NaCl are presented. The two strong, negative bands at 208 nm and 222 nm, and one positive band at 193 nm, were characteristic for α-helical structures, while the bands located at 218 nm (negative) and 195 nm (positive) corresponded to a well-defined β-sheet [43,44].

The results show no significant structural changes under the selected experimental conditions, which indicated that lysozyme is stable over a wide range of pH. Based on spectral deconvolution, the conformational composition of lysozyme was estimated. It consisted of 36% α-helix, 31% – β-sheets, 1% – β-turn, and 32.0% random structures. However, in the literature, it was found that changes in the lysozyme conformation depended on the environmental conditions. The secondary structure content of this protein for different types of environments is presented in Table TS1. It is also known that under extreme environmental conditions, lysozyme is even considered to be an amyloidogenic molecule [45].

Table 1
Potential sequences in the negative- and positive-going potential scans applied to the lysozyme modified Au electrode in electrolyte solutions of different pD values in situ PM IRRAS experiments.

pD	potential sequence in the negative-going potential scan/V	potential sequence in the positive-going potential scan/V
4.0	0.3, 0.2, 0.05, −0.05, −0.1, −0.2, −0.3	−0.2, −0.1, −0.05, 0.05, 0.2, 0.3, 0.4
7.5	0.3, 0.2, 0.1, 0.0,-0.2, −0.4	−0.2, 0.0, 0.1, 0.2, 0.3, 0.4
9.0	0.0,-0.1, −0.2,-0.4, −0.5, −0.6, −0.7	−0.6, −0.5, −0.4, −0.2, −0.1, 0.0, 0.05



Scheme 1. Structure of lysozyme molecule. α-helices are shown in blue, β-sheets in red, and β-turns in yellow.

In Scheme 2, the distribution of positively and negatively charged domains (positive - blue, negative - red, neutral - white) on the lysozyme surface and the dipole moment value (p) of the molecule under selected conditions corresponding to pH = 4, 7.5, and 9 are presented. Visualisation was prepared using the 1iee structure from the RCS protein database in the PyMOL software package (DeLano Scientific LLC, CA, USA). The resulting models show that the charge distribution on the lysozyme surface is asymmetrical. Kubiak et al. demonstrated that the most positively charged areas are located at the N, C-terminals, and opposite sides. In the middle, there are both positively and negatively charged areas [41]. It can be expected that during the adsorption process, a negatively charged gold surface will prefer contact with positively charged residues by electrostatic attraction, so it can be predicted that molecular structures near the N, C-terminal may be the most exposed to conformational deformations. Observations compatible with these assumptions have been confirmed by Wei et al. They showed that interactions between lysozyme and negatively charged polyethylene surface mainly affect the α-domain, which contains the C-terminal, while the β-domain was preserved [46]. Below, we describe the study results on the effect of the net surface-charge density on the secondary structure of adsorbed lysozyme.

3.2. Lysozyme adsorption onto the gold surface

To determine the nature of the interactions between lysozyme and the gold surface, the mass of adsorbed protein was established depending on the zeta potential of lysozyme molecules. The values

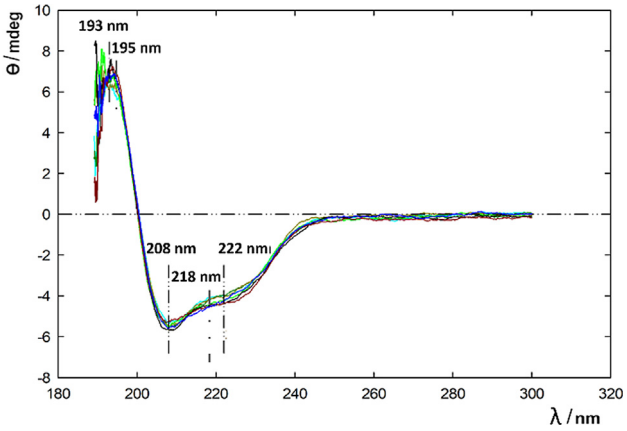
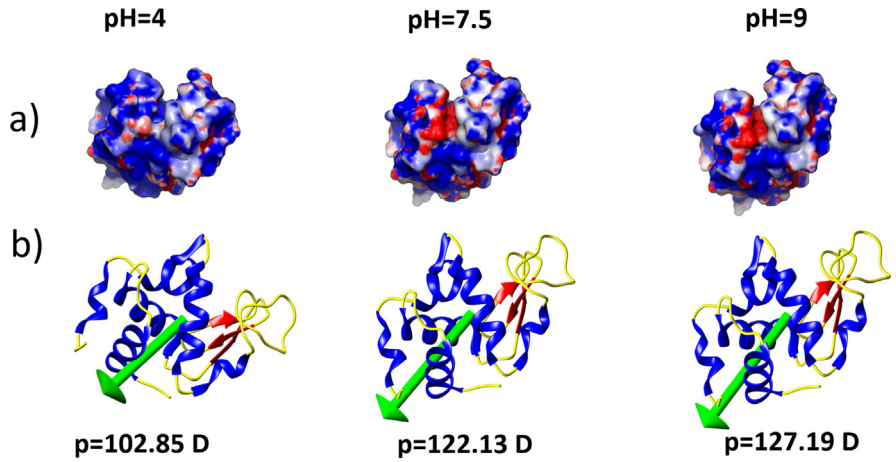


Fig. 1. CD spectra of lysozyme in solutions at ionic strength I = 0.01 M NaCl. Each curve corresponds to a different pH in the range of 3.0–11.0.



Scheme 2. Visualization of a) the charge distribution on the surface of the lysozyme (positive charge - blue, negative - red, neutral – white) and b) the dipole moment of each lysozyme molecule, depending on the pH for I = 0.01 M NaCl, is marked by a green arrow (p corresponds to the dipole moment value).

of zeta potential we have previously reported [47] and the isoelectric points of lysozyme and the gold sensor were 10.0 and 3.4, respectively. The mass of the protein layer adsorbed on the gold surface ($\Gamma_{QCM\text{-}D}$) was investigated using a quartz crystal microbalance with dissipation monitoring (QCM-D). According to the following scheme, the measurement series were carried out: solvent baseline (10 min 0.01 M NaCl), 90 min adsorption of lysozyme (100 ppm, 0.01 M NaCl), rinsing with a 0.01 M NaCl solution for 90 min. The values of the adsorbed mass and zeta potential of the lysozyme molecules as a pH function are presented in Fig. 2a and b, respectively.

These studies were carried out at open circuit potential. The minimum adsorbed mass ($\Gamma_{QCM\text{-}D}$ = 335 ng cm^{-2}) occurred when lysozyme had the highest zeta potential of 43 mV at pH = 4.0. This means that the surface tended to compensate for the charge by lysozyme adsorption, but the repulsion between protein molecules in the adsorption layer was high. When lysozyme had a lower positive charge, the repulsive interactions in the layer were smaller, and consequently, a larger number of protein molecules could be adsorbed on the metal surface. As the pH increased, the zeta potential of the protein decreased, the mass of the adsorbed layer increased, and thus, the surface coverage. At the isoelectric point (i.e.p.), when repulsion between the protein molecules was minimal, maximum adsorption was observed (620 ng cm^{-2} at pH = 10). The measurements showed that electrostatic interactions played a major role in effectiveness of the lysozyme adsorption on the gold surface. The mass of the adsorbed protein progressively increased from 335 ng cm^{-2} at pH 4.0 to 620 ng cm^{-2} at pH 10.0, due to the concurrent, gradual decrease in charge of the protein molecule. The trends in the binding affinity and the surface saturation amount correspond well with the degree of change of protonation of the adsorbed molecules. Similar behaviour of lysozyme was observed during adsorption on the silica surface and analysed both by experiment and computer simulations [41]. As the lysozyme is ellipsoidal in shape [40], it may be oriented differently on the surface. Three major orientations of proteins have been defined: *side-on* when the angle between the long axis of the protein molecule and the surface is in the range of 0–30°, *end-on* – the angle is from 60° to 90°, and in *between*, which is an intermediate state of the *side-on* and *end-on* positions (the long axis of lysozyme and the surface form an angle in the range of 31–59°) [41]. According to previous calculations based on the random sequential adsorption (RSA) model full monolayer in orientation *side-on* is achieved when the adsorbed mass measured by QCM-D

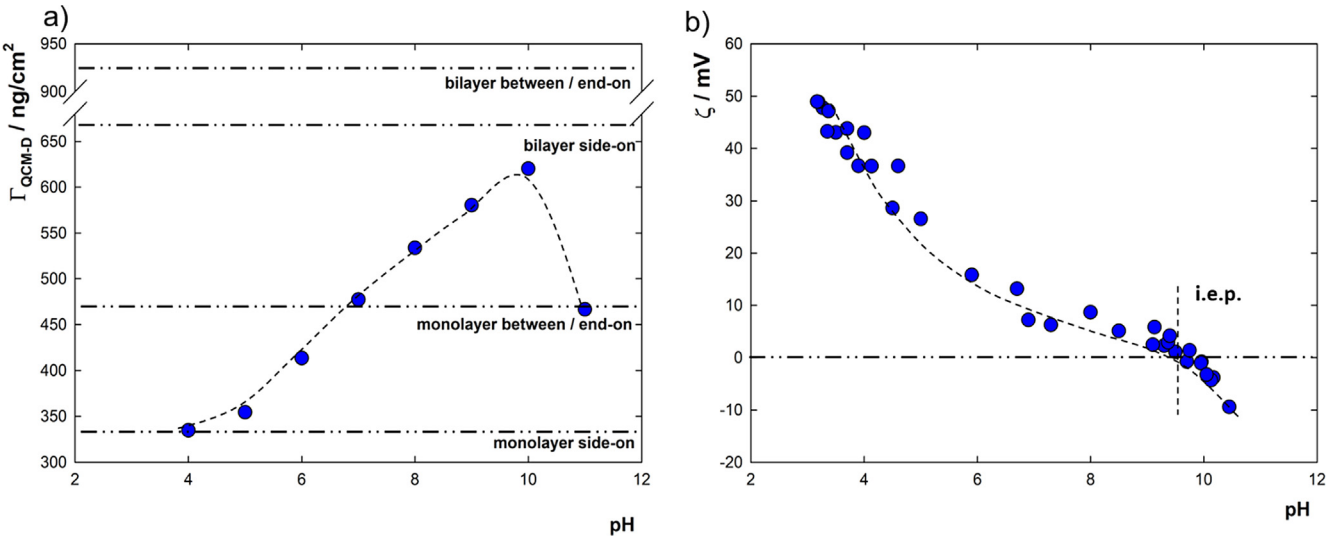


Fig. 2. a) Mass of adsorbed lysozyme molecules ($\Gamma_{QCM\text{-}D}$) at a concentration of 100 ppm from I = 0.01 M NaCl on the Au surface monitored using the QCM-D method, b) zeta potential of lysozyme dependent on pH.

($\Gamma_{QCM\text{-}D}$) is equal to 330 ng cm^{-2}; a higher mass up to 467 ng cm^{-2} indicates reorientation of molecules to *between/side-on* positions [47]. Our experimental data showed that a monolayer in *between/side-on* orientation was formed in pH = 4 to 7. In solutions with pH > 7, more molecules began to associate, starting to build a bilayer. In pH = 11, after crossing the isoelectric point, the weaker interactions translated into lower effectiveness of adsorption, but still, monolayer in *between/end-on* orientation was achieved.

3.3. Effect of the electric potential of the gold surface on the lysozyme adsorption

Lysozyme was adsorbed on a polycrystalline Au surface from 0.01 M NaCl solution at pH 4.0, 7.5, and 9.0. The protein adsorption experiments were carried out at different potentials applied to the Au electrode. In one series of experiments, the adsorption potentials were set to E_{ads} = 0.35 V at pH = 4, E_{ads} = 0.30 V at pH = 7.5 and E_{ads} = 0.00 V at pH 9. These adsorption potentials corresponded to 15 μC cm^{-2} surface charge density of the unmodified Au electrode. These potentials are more positive than the potential of zero charge (E_{pzc}) of the Au electrode in the respective electrolyte solutions. Under these conditions, Cl^- (solutions with pD = 4 and 7.5) as well as OD^- ions (pD = 9) were adsorbed on the Au surface [45,46]. Fig. S1 shows the capacitance potential plots of the Au surface with lysozyme films. A decrease in the capacitance confirmed adsorption of the protein in the metal surface. The potential driven desorption of the protein film from the Au surface was not determined. To find our about the structural details of adsorbed protein films, PM IRRA spectra in amide I and amide II modes regions were recorded and are shown in Fig. 3a. In the second series of experiments, the adsorption potentials equalled E_{ads} = −0.2 5 V at pH 4, E_{ads} = −0.35 V at pH = 7.5, and E_{ads} = −0.65 V at pH = 9. They corresponded to the surface charge density of 10 μC cm^{-2} of the unmodified Au electrode and were more negative than the E_{pzc} of a polycrystalline Au electrode in NaCl and NaOH solutions [49]. The corresponding PM IRRA spectra of lysozyme films adsorbed on the Au surface are shown in Fig. 3b.

Lysozyme gave three absorption modes in the 1750–1350 cm^{-1} spectral region (Fig. 3). The strong and broad absorption mode, centred at 1650 cm^{-1}, was assigned to the amide I' mode. It was overlapped by another broad mode ~1580 cm^{-1}. This mode had a complex composition, and contained a contribution from the amide II mode [predominantly $\delta(NH_2)$ in isotopically unsubstituted amide groups] [50], and $\nu_{as}(COO^-)$ in the side chains of the protein. This result indicated that in the lysozyme film adsorbed on the Au surface, some fraction of amide hydrogens were protected and did not undergo isotopic exchange with D_2O and OD^- ions from the electrolyte solution. Indeed, lysozyme molecules in the solution phase showed that ca. 50% of their amides were protected in neutral solutions, while only 11% were in alkaline solutions (pD = 9.5) [51]. To the mode centred ~1450 cm^{-1} contribute the amide II' mode [predominantly $\delta(ND_2)$ in isotopically substituted amide groups]. On the low wavenumber side, this mode was overlapped by the $\nu_{as}(COO^-)$ mode. In PM IRRA spectra of lysozyme films adsorbed at $E_{ads} > E_{pzc}$, a fourth IR absorption mode at 1710 cm^{-1} was present (Fig. 3a). Fig. 3 shows an increase in the intensities of that the IR absorption modes of lysozyme with the increase in the pD of the electrolyte solution. Larger amounts of the protein were adsorbed on the Au surface in alkaline than in acidic solution. This result agrees with the QCM-D studies of lysozyme adsorption at open circuit potential described above and previous reports [41,47,52–56,57]. In addition, Fig. 3a shows that in films adsorbed at positive net charges of the Au surface, the intensities of IR absorption modes of the protein were around one order of magnitude larger than in films prepared at negative net charges of the metal surface (Fig. 3b). At positive net charge densities of the

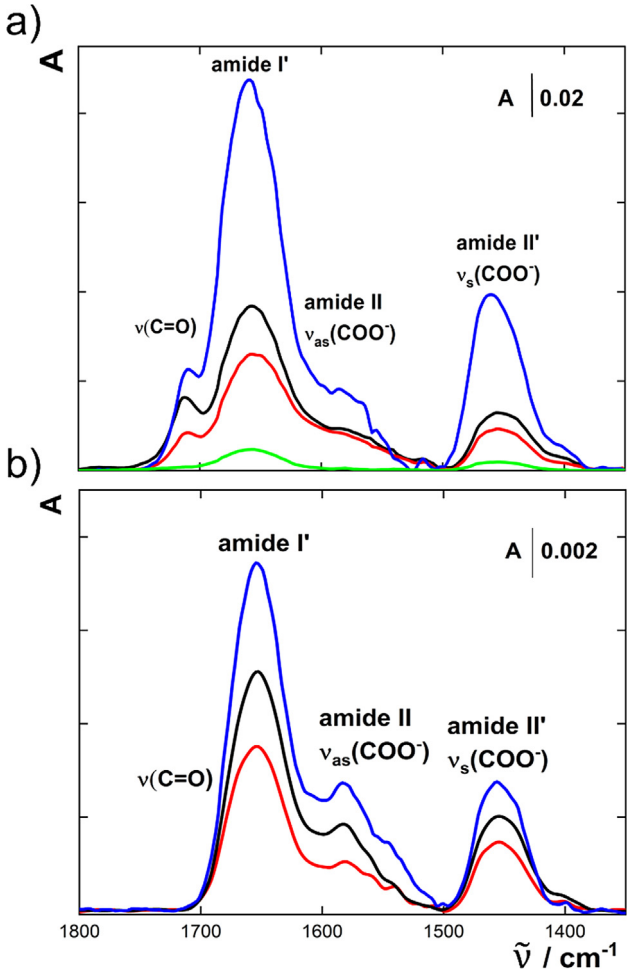


Fig. 3. In situ PM IRRA spectra in 1800–1350 cm^{-1} region at E = 0.0 V of freshly prepared lysozyme films on the gold surface in D_2O solutions at the following adsorption potentials and pD values a) $E > E_{pzc}$: E_{ads} = 0.35 V at pD = 4 (red line); E_{ads} = 0.30 V at pD = 7 (black line) and E_{ads} = 0.00 V at pD = 9 (blue line) and from 0.01 M NaF in D_2O (pD = 7) solution at E_{ads} = 0.30 V (green line) b) $E < E_{pzc}$: E_{ads} = −0.25 V at pD = 4 (red line); E_{ads} = −0.35 V at pD = 7 (black line) and E_{ads} = −0.65 V at pD = 9 (blue line).

substrate, enhanced adsorption of positively charged lysozyme molecules was observed. This result appears to be counterintuitive. However, the adsorption of lysozyme from 0.01 M NaF solution (pH = 7.5) at E_{ads} = 0.30 V (at $E_{ads} > E_{pzc}$) gave an IR spectrum with intensities of the amide I mode similar to lysozyme films adsorbed at $E < E_{pzc}$ (Fig. 3a, green line). The F^- ions do not adsorb specifically on the Au surface [48], thus are suitable for electrochemical studies. However, F^- ions are not biocompatible and may destabilize the protein structure and conformation [53]. Clearly, specifically adsorbed anions facilitated electrostatic interactions with positively charged lysozyme molecules and reduced the electrostatic repulsions between adsorbed lysozyme molecules, yielding a thick protein film. This observation agrees with a recent molecular simulation, which predicted that the adsorption of Cl^- ions on a charged interface reduces the electrostatic interactions between lysozyme and screens the positive charge of the solid substrate [58]. In addition, experimental studies of the electroadsorption of lysozyme at an aqueous-organogel interface, at a positive potential bias to the interface, was accompanied by the transfer of the organic anions at the interface and led to enhanced adsorption of lysozyme, compared to the negative potential bias [59]. A large surface concentration of the adsorbed anions and/or formation of

a thick protein film led to significant changes in the lysozyme spectrum's shape. The ν(C=O) mode was assigned to the C=O stretching modes in the denatured protein (Fig. 3a). Below, we discuss the stability, secondary structure, and conformation of lysozyme in films adsorbed on the Au electrode surface.

3.4. Lysozyme films adsorbed at positive electric potentials applied the gold electrode

In the lysozyme film prepared from 0.01 M NaCl solution at pH = 9, significant spectral changes were observed in the first potential cycle (Fig. 4a). In the first half cycle, in the negative-going potential scan, at $0.15 \leq E \leq -0.40$ V, no spectral changes were observed (Fig. 4a). In this potential region, the hydroxide ions were adsorbed on the Au surface. However, at $E \leq -0.6$ V, an irreversible decrease in the intensities of all IR absorption modes of lysozyme occurred. At these potentials, the OD^- ions desorbed from the Au surface[46], destabilizing the adsorbed protein film. In the successive half cycle, in the positive-going potential scan (Fig. 4a), the intensities of the IR absorption modes of lysozyme further decreased, reaching a steady-state value in the next successive 2nd-6th scans (Fig. 4b). To investigate changes in the amount and conformation of adsorbed lysozyme, a 2-dimensional correlation spectroscopy (2-DCS) analysis was carried out (Fig. S2). In the synchronous spectrum shown in Fig. S2, all cross peaks were positive, indicating that these three IR absorption mode intensities changed similarly.

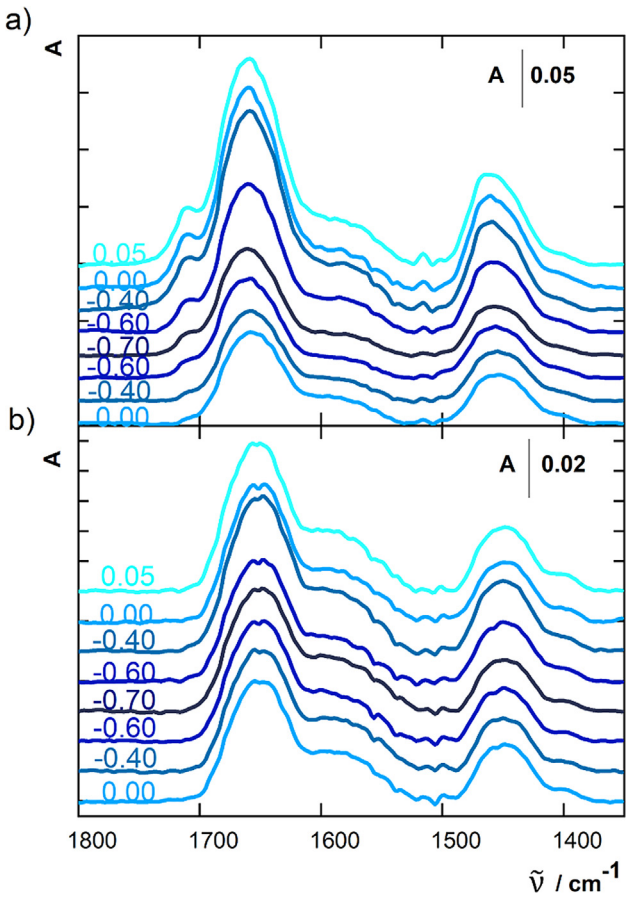


Fig. 4. PM IRRA spectra in the 1800–1350 cm^{-1} spectral region of the lysozyme film adsorbed at E_{ads} = 0.0 V from 0.01 M NaCl + NaOD in D_2O solution (pD = 9) in the a) first and b) successive (2nd–6th) negative and positive-going potential scans at the potentials marked in the figure.

A simultaneous and irreversible decrease in the intensities of the IR absorption modes of lysozyme indicated that in the first potential cycle, some protein molecules desorbed from the Au surface. The intensity of the ν(C=O) mode at 1708 cm^{-1} decreased to zero. Thus, at $E > E_{pzc}$ the OD^- ions desorption, facilitated desorption of denatured protein molecules which diffused into the electrolyte solution. In the successive (scan 2nd to scan 6th) potential cycles, the IR absorption modes' intensities did not change irreversibly. Instead, some variations in the amide I mode's intensity between negative and positive potentials were observed. Fig. 5 shows asynchronous and synchronous correlation spectra of the lysozyme film during the potential cycling.

The asynchronous spectrum was used to deconvolute overlapped IR absorption modes [60,61]. The spectrum in Fig. 5a showed cross peaks of the modes at 1466, 1578, 1598, 1606 and 1629 $cm^{-1,}$ which were correlated to IR absorption mode at 1675 cm^{-1}. The asynchronous spectrum showed that few bands compose the amide I' mode. During the potential scan, some non-simultaneous changes occurred in the lysozyme conformation and/or orientation. The deconvolution of the PM IRRA spectra based on the second derivative and FSD (Fourier self-deconvolution) procedures yielded IR absorption modes centred at: 1400, 1440, 1468, 1515, 1550, 1568, 1586, 1605, 1627, 1643, 1659, and 1678 cm^{-1} (Fig. S3). The positions of these modes corresponded to the bands found in 2D correlation spectra. Based on the deconvolution procedures described above, the PM IRRA spectra were deconvoluted at each potential applied to the Au electrode. A deconvoluted IR absorption spectrum of the lysozyme film adsorbed from solution with pD = 9, at E_{ads} = 0.0 V is presented in Fig. 6. The amide I' mode provides information about the conformation and composition of secondary structural elements of proteins [62,63].

The amide I' mode of lysozyme was deconvoluted into five components, indicating a complex secondary structure of this protein. The IR absorption mode at 1678 cm^{-1} was assigned to β-turns. The IR absorption mode around 1660 cm^{-1} was the strongest in the spectrum and originated from helical structural elements. The position of this mode was dependent on the potential applied to the Au electrode (Fig. S4). At both negative and positive potentials, this mode was centred at 1659.5 cm^{-1} and shifted to 1662 cm^{-1} at $-0.4 < E < -0.2$ V. Thus, the hydration of α-helices changed during the potential scan. In general, the position of the α-helix amide I' mode was high, indicating a relatively weak strength of hydrogen bonds formed to the helices. The hydration changes observed here at α-helices might have affected the number of hydrogen bonds formed along the helices and thus their structure. A molecular-dynamics simulation study predicted that the unfolding of α-helices in lysozyme molecules would involve progressive hydration by inserting water molecules in their hydrogen-bond network [42]. Insertion of water into the helix structure could facilitate the isotopic exchange in this protein fragment. The synchronous spectrum showed cross peaks at (1450, 1660) cm^{-1} and (1571, 1645) cm^{-1} (Fig. 5b).

The cross peak at (1450, 1660) cm^{-1} correlated the amide II's changes with changes in the helical protein fragments. Lysozyme fragments with an α-helical structure were not protected and underwent isotopic substitution of their NH_2 groups by D atoms. The 3_{10}- and α-helices have been proposed as intermediate products during the α-helix-to-random coil transition [64]. In conclusion, our results showed that in the alkaline solution, the structure of the α-helices in the adsorbed lysozyme film was disrupted and contained different helical structures. The IR absorption mode centred at 1642 cm^{-1} was assigned to random coils, and the mode at 1627 cm^{-1} to β-sheet structures:

The presence of a broad IR absorption mode around 1610 cm^{-1} confirmed the presence of aggregated β-sheet structures (amyloid-

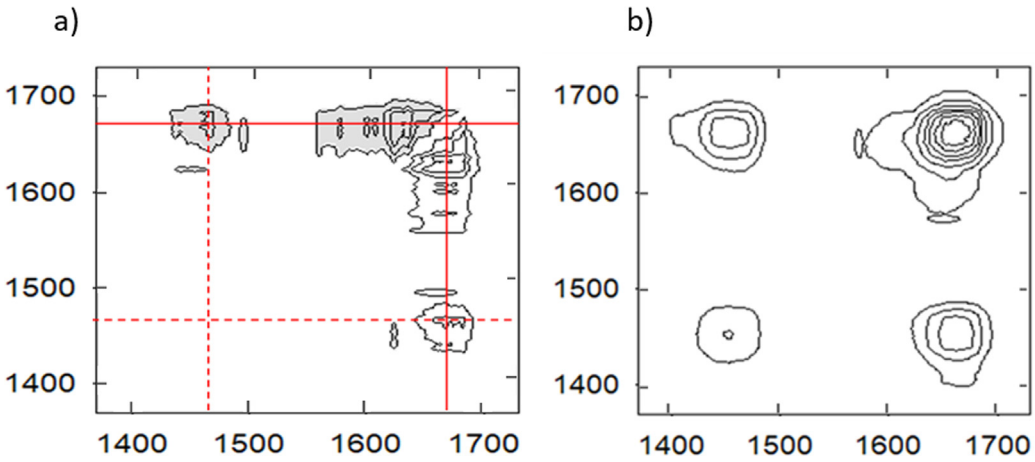


Fig. 5. a) Asynchronous and b) synchronous 2D-correlation spectra of the lysozyme film adsorbed from 0.01 M NaCl + NaOD solution, pD = 9, on the Au surface at E_{ads} = 0.0 V in the successive (2nd–6th) potential scans.

like) [65–69]. The amide I' mode's deconvolution indicated that α-helices, β-sheets, β-turns, and random secondary structural elements contributed to the lysozyme structure. These structural elements were found in lysozyme dissolved in solution phase [47,70–74] and in crystal form [75–77]. The presence of aggregated β-sheets was characteristic for the adsorbed state of lysozyme. Furthermore, integral intensities of the amide I' modes were used to estimate each secondary structural element's content in the lysozyme film (Fig. 7). Fig. 7 shows that the content of α-helices varied between 32% at negative to ca. 36% at positive potentials. The content of random structures was close to 20–24%. The β-sheet structural elements existed in the native and aggregated forms, and the content range of both β-sheet structures was close to 15%. β-turns composed ca. 16–18% of the secondary structural elements. The X-ray (or NMR) resolved structure of hen egg-white lysozyme (1iee) provided the following composition of the secondary structural elements in the protein: 41% α-helices, 10% β-sheets, 21% β-turns, and 28% disordered structures [78]. According to the literature, in the solution phase, the content of α-helices is close to 30–40%, β-turns to 25%, random structures 25–30%, and β-sheet to 10–20% [47,70–74]. Our analysis indicated a decrease in the content of random coil structures.

The aggregated β-sheet structures could thus arise from conformational changes of the random fragments. In the lysozyme films adsorbed at $E > E_{pzc}$ from 0.01 M NaCl solutions at pH = 7.5 and 4, no potential-dependent changes in the PM IRRA spectra were observed (Figs. S5 and S6). The second derivative and FSD were used to deconvolute the IR absorption modes of lysozyme. The deconvoluted spectra of lysozyme films are shown in Fig. 8. Deconvolution of the amide I' mode of lysozyme in films adsorbed from acidic solutions gave the same results as from alkaline solutions, as described above (Fig. 8a). Spectral changes were observed in the protein film adsorbed from neutral solution (Fig. 8b).

A new band, assigned to 3_{10}-helices, appeared at 1677 cm^{-1}, while the absorption maximum of α-helices appeared at 1652 cm^{-1}. The pH of the electrolyte solution had an impact on the α-helical protein fragments. In neutral solutions, the α-helices were well hydrated. However, their content decreased to ca. 25%, while the 3_{10}-helices composed ca. 15% of the lysozyme secondary structural elements (Table 2, Fig. S7). The total content of helices in lysozyme films is comparable with their content in

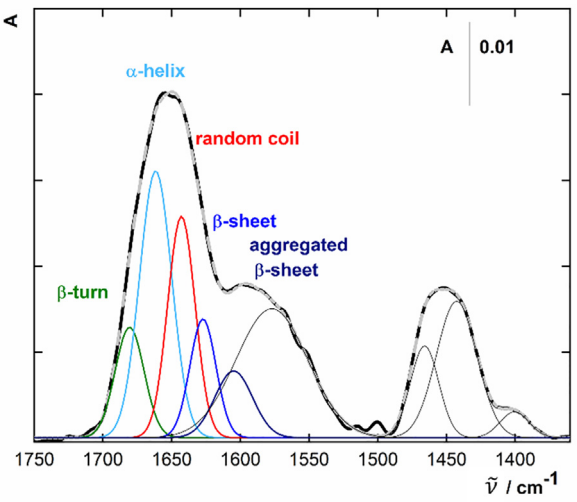


Fig. 6. Deconvoluted PM IRRA spectrum of a lysozyme film adsorbed on the Au surface at E_{ads} = 0.0 V in 0.01 M NaCl, in D_2O at pD = 9 in the successive (2nd-6th) potential scans at E = 0.0 V.

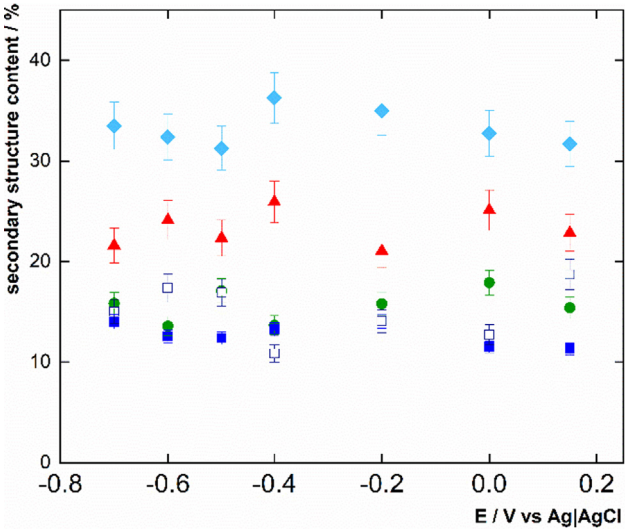


Fig. 7. Percent content of the secondary structure elements in lysozyme adsorbed from 0.01 M NaCl + NaOD, pD = 9 at E_{ads} = 0.0 V as a function of the potential applied to the Au electrode. Symbols representation: (●, green) – β-turn, (◆, light blue)- α-helix, (▲, red)- random coil, (■, blue) – β-sheet, and (□, dark blue) – aggregated β-sheet.

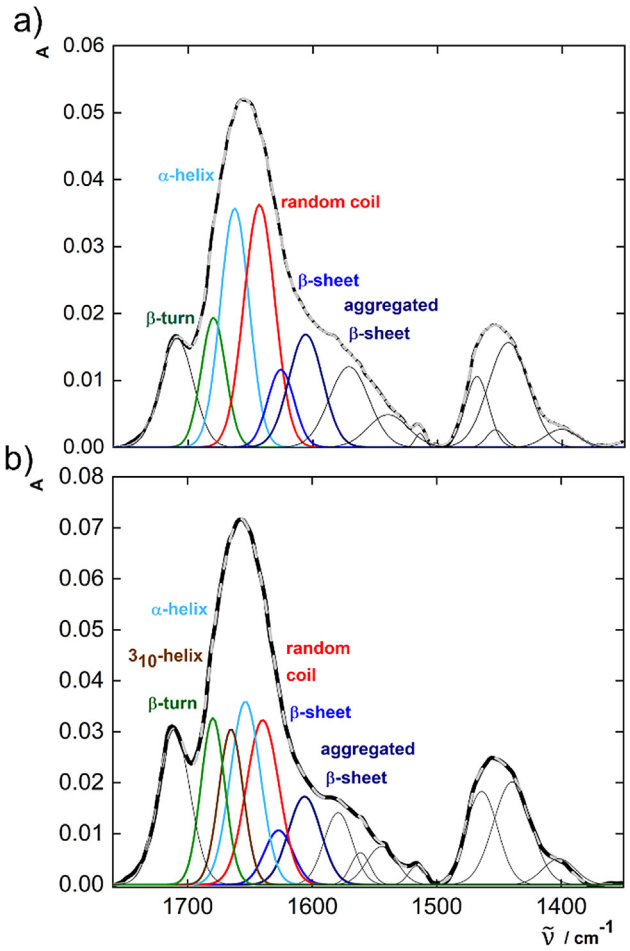


Fig. 8. Deconvoluted in-situ PM IRRA spectra in the 1780–1380 cm^{-1} spectral region of the lysozyme films on the Au surface adsorbed from 0.01 M NaCl aqueous solutions a) at pH = 4 and E_{ads} = 0.35 V at E = 0.05 V, and b) pH = 7.5 and E_{ads} = 0.00 V at E = 0.1 V. In-situ experiments were carried out in 0.01 M NaCl in D_2O at pD corresponding to the adsorption conditions. pD was adjusted by addition of either DCl or NaOD.

the solution phase (30–40%) [47,70–74]. In neutral solution, a certain number of α-helices underwent a conformation change to 3_{10}-helices. In alkaline and acidic solutions, this process was less prominent. The amide I' mode appeared in the range 1659–1662 cm^{-1} and indicated a disruption of the α-helix structure, and significant changes of their hydration/hydrogen-bond network, suggesting the existence of other helical structures such as 3_{10}- or π-helices [64]. Compared to the solution phase, in lysozyme films, the content of β-turns decreased by ca 10%, while that of the random coils by only a few percent. Simultaneously, the content of aggregated β-sheet structures increased to 12–18%. The content of native β-sheet structures in lysozyme in the adsorbed state and in the solution phase was ~10–15%. These results indicated that β-turns and random coils favoured a conformational transition to aggregated β-sheet structures. This transition was more pronounced in alkaline and acidic solutions than in neutral solutions (Tables 2 and TS1).

Since the specific adsorption of anions on the Au surface seemed to have an effect on the stability and structure of lysozyme films, the PM IRRA spectra of the lysozyme film prepared from the NaF solution (pH = 7.5), in the absence of the specific anion adsorption, were carefully analysed. Fig. 9 shows in situ PM IRRA spectra of the protein films, in the first potential cycle, both in negative and positive-going potential scans.

The intensities of the amide I and II modes decreased slightly during the first potential scan. Further potential cycling led to gradual decrease in the intensities of all IR absorption modes, indicating a slow dissolution of the protein film. Interestingly, in the first potential scan, at positive potentials, a shoulder at the high wavenumber side of the amide I mode, ~1710 cm^{-1} was present in the PM IRRA spectra. By contrast, at negative potentials, the intensity of the $\nu_{as}(COO^-)$ mode at 1574 cm^{-1} increased and the shoulder around 1710 cm^{-1} disappeared from the spectra (Fig. 9). These spectral features indicate potential-dependent changes in the protonation state of side chain carboxylic groups in glutamic and aspartic acid amino acids, and thus local potential-dependent changes in pD. In a freshly prepared lysozyme film, the deconvolution of the amide I mode gave IR absorption bands at 1678 cm^{-1} (β-turns), 1669 cm^{-1} (3_{10}-helices), 1656–1651 cm^{-1} (α-helices), 1640 cm^{-1} (random coils), 1626 and 1601 cm^{-1} (native and aggregated β-sheets). Similar to films prepared from neutral NaCl solution, in NaF solution, the 3_{10}-helices were present in the adsorbed lysozyme molecules. The position of the amide I mode of α-helices were dependent on the electrode potential and shifted from 1656 cm^{-1} at E = −0.4 V to 1651 cm^{-1} at E = 0.3 V. Thus, the hydration of the helical structural elements changed as a function of the electrode potential. Since in the electrolyte solution containing F^- the protein film was unstable over long time potential cycling, the specific adsorption of Cl^- seems to be biologically relevant for stabilisation of the lysozyme films.

3.5. Lysozyme films adsorbed at negative electric potentials applied the gold electrode

Deconvoluted in situ PM IRRA spectra of lysozyme films adsorbed at net negative potentials applied to the Au electrode, are shown in Fig. 10. The number and position of the IR absorption modes contributing to the amide I' mode depended on the pH of the electrolyte solution from which the protein film was adsorbed. β-turns gave the amide I' mode at 1683–1678 cm^{-1}. The most significant spectral changes were observed for the helical structures. In films prepared from acidic solutions, this mode was centred at 1656 cm^{-1} and corresponded to intact α-helical structures. In neutral solutions, as observed previously, a splitting of this mode was observed. The α-helices gave an IR absorption at 1653 cm^{-1} and the 3_{10}-helices at 1667 cm^{-1}. In alkaline solutions, these two modes merged to provide an IR absorption mode at 1661 cm^{-1}.

Table 2
Average percent content of the secondary structure elements in lysozyme adsorbed at net positive potentials from 0.01 M NaCl at pH = 4, 9 and 7.5.

pD of the electrolyte solution	content of secondary structure elements in lysozyme films/%					
	β-turn	3_{10}-helix	α-helix	random coil	β-sheet	aggregated β-sheet
4.0	15	0	31	29	9	16
7.5	16	13	25	24	10	12
9.0	~5*	0	~33*	23	14	15

* Potential dependent content, average values are given in the table.

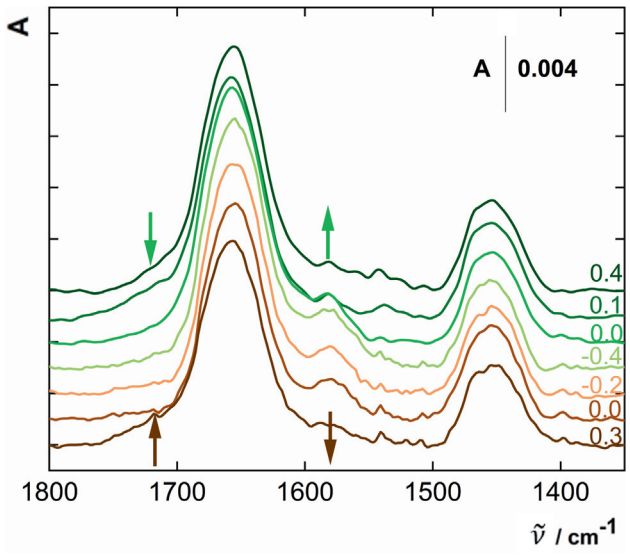


Fig. 9. PM IRRA spectra in the 1800–1350 cm^{-1} spectral region of the lysozyme film adsorbed at E_{ads} = 0.3 V from 0.01 M NaF in D_2O solution (pD = 7.5) in the first potential cycle in the negative (green) and positive-going (brown) potential scans at the potentials marked in the figure. Arrows show the directions of the IR absorption modes changes.

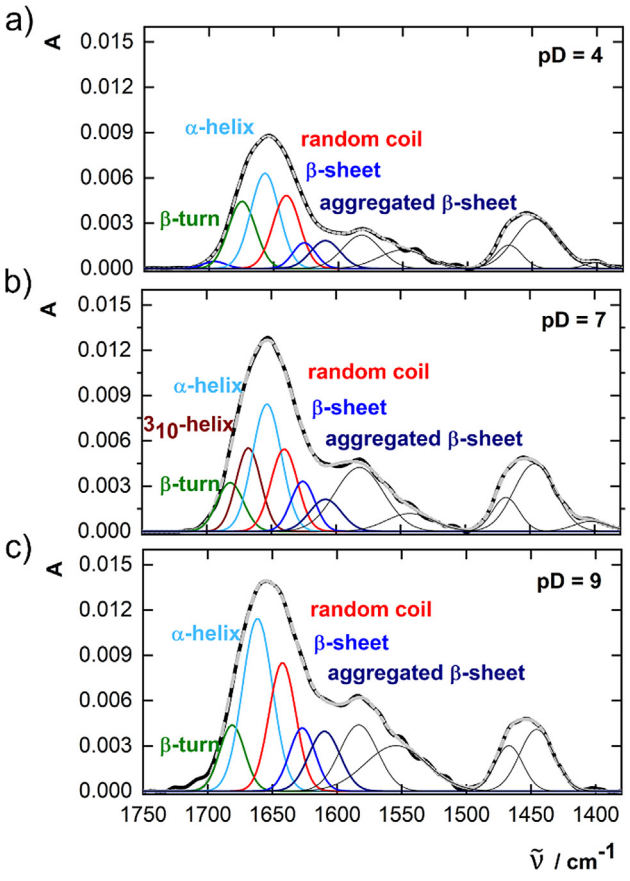


Fig. 10. Deconvoluted in situ PM IRRA spectra in the 1750–1380 cm^{-1} spectral region of the lysozyme films on the Au surface fabricated in 0.01 M NaCl aqueous solutions a) at pH = 4 and E_{ads} = −0.25 V at E = 0.05 V, b) pH = 7.5 and E_{ads} = −0.35 V at E = 0.1 V, and c) pH = 9 and E_{ads} = −0.65 V and E = −0.20 V. In situ experiments were carried out in 0.01 M NaCl in D_2O at pD corresponding to the adsorption conditions. pD was adjusted by addition of either DCl or NaOD.

Table 3
Average percent content of the secondary structural elements in lysozyme adsorbed at net negative potentials from 0.01 M NaCl at pH = 4, 9 and 7.5.

pD of the electrolyte solution	content of secondary structure elements in lysozyme films/%					
	β-turn	3_{10}-helix	α-helix	random coil	β-sheet	aggregated β-sheet
4.0	20	0	36	22	12	10
7.5	11	18	30	19	10	12
9.0	21	0	39	18	9	13

Thus, the environment from which lysozyme adsorbs on the Au surface affects the hydration and structure of helices. The amide I' mode of random coils was centred at 1640 cm^{-1}. β-sheets gave a main IR absorption mode at 1626–1627 cm^{-1} and a weak IR mode at 1696 cm^{-1}. This result indicates the presence of antiparallel β-sheet structures.

The deconvoluted amide I' modes were used to calculate the content of different secondary structural elements in the lysozyme films (Fig. S8). These results are collected in Table 3. In films adsorbed at negative potentials applied to the Au electrode, the content of helical structure elements was higher (35–50%) than in the films adsorbed at applied positive potentials. It remained at the physiological level. The content of β-turns was, by a few percent, lower than in the solution phase, while the content of random coils decreased by 5–10%. The content of native β-sheet structures was 8–11%, while the content of aggregated β-sheets was on the level of 10–14%. These results indicated that native β-sheets and random coils might transition to aggregated β-sheet structures. In alkaline solutions, this process seemed to be more accessible than in neutral solutions. In neutral solutions, the structure of α-helices was affected. Changes in the hydrogen-bond network in these protein fragments led to the formation of 3_{10}-helices.

4. Conclusions

Our results showed that both the pH of the electrolyte solution, electric potentials, and the presence of specifically adsorbed ions determined the amount and the secondary structure of lysozyme adsorbed on the gold electrode surface. Independently of the potential applied to the Au electrode, the amount of the adsorbed lysozyme increased with an increase in the electrolyte solution's pH. Our results confirmed that a decrease in the surface charge density on the lysozyme molecule facilitated lysozyme accumulation at interfaces. Electrostatic interactions and the surface charge density on the metal surface further affected the amount of adsorbed protein. In protein films formed at $E_{ads} > E_{pzc}$, the specific adsorption of anions screened the lysozyme molecules' positive surface charge. In consequence, a large amount of the protein adsorbed onto the Au surface. However, in these densely packed, thick films, denaturation of some protein molecules was observed. The protein film displayed limited stability in films prepared in the presence of OH^- and F^- ions. Thus, the specific adsorption of biologically relevant Cl^- is important for the stabilisation of the protein film. At net negative surface charge densities ($E_{ads} < E_{pzc}$), no anions were adsorbed on the Au surface, and therefore the number of adsorbed protein molecules was significantly lower.

Except for the amount of the adsorbed protein, the substrate surface-charge density had a negligible effect on the conformation and structure of the adsorbed protein. However, the environment (pH) of the solution from which the protein was adsorbed significantly impacted the lysozyme structure. In acidic and alkaline

media, α-helices gave the amide I' mode in the 1656–1662 cm^{-1}, indicating that helical protein fragments were weakly hydrated in the adsorbed lysozyme/or the hydrogen-bond network in this protein fragment had changed. Hydration changes led to a partial loss of the α-helix structure. Other helical structures, such as 3_{10}- and α-helical fragments, coexisted along α-helices.

In a neutral medium, the process of α-helix disruption seems to occur according to a different mechanism. The amide I' arising from helical structures had two maxima at 1667 cm^{-1} (3_{10}-helices) and 1653 cm^{-1} (α-helices). The presence of two amide I' modes indicated that some helices had a pure 3_{10}- while others had a pure α-helix structure. Other structural elements, β-turns, random coils, and β-sheets, were able to undergo a transition to an aggregated β-sheet structure. It is indeed confirmed by the 2-DCS analysis, which showed that 1606 cm^{-1} (aggregated β-sheets) and 1629 cm^{-1} (native β-sheets) were correlated to the IR absorption mode at 1675 cm^{-1} (β-turns) (Fig. 5a). The amount of aggregated β-sheets was higher in films fabricated at net positive charges of the Au electrode ($E_{ads} > E_{pzc}$). Under these conditions, the surface concentration of specifically adsorbed anions on the Au electrode surface was high (few to several M) [79–81]. Thus, electrostatic interactions between adsorbed anions and the adsorbing lysozyme facilitated agglomeration of the protein on the Au surface. A high surface concentration of both adsorbed anions and lysozyme led to conformation changes in the adsorbed protein. These changes were expressed in two ways:

(i) Increase in the content of aggregated β-sheet structures
(ii) Denaturation of a fraction of adsorbed lysozyme molecules.

With an increase in the pH (pD) of the electrolyte solution, we observed a decrease in the stability of the protein film. It was associated with the fact that the surface-charge density on lysozyme molecules decreased with a pH increase, leading to reduced electrostatic interactions with anions adsorbed on the Au surface. In conclusion, the process of conformational changes in lysozyme involved two parallel processes. One involved changes in the hydration/hydrogen bond network at helices, yielding diverse helical structures (α-, 3_{10}- and/or π-helices). According to the literature, these changes in helices' structure may finally lead to the formation of β-turns and random coils [64]. In the second process, other structural elements (β-turns, β-sheets and random coils) displayed an ability to form aggregated β-sheet structures (amyloid-like structures). Indeed, molecular dynamics studies predicted two pathways of the lysozyme unfolding/folding process [42]. The two domains: β-rich in β-sheet and α-rich in α-helix structures displayed different unfolding pathways [42,51,82,83]. Our results indicate that two parallel processes occurring at helices and other structural elements contribute to structural changes in lysozyme films on the Au surface. In this work, we illuminate the phenomena accompanying electrical potential-dependent changes involved in the protein misfolding process.

When proteins come in contact with solids, they adsorb on their surfaces. The protein properties, surface properties, electrolyte solution (composition, ionic strength and pH), and environment of the sample (temperature, pressure) affect the protein adsorption porcess. Our results show that even the structure and conformation of a hard protein, such as lysozyme, is affected by the substrate properties and the electrolyte solution composition. Not only the charge of the substrate but the ability of counterions interacting electrostatically with protein molecules to accumulate (adsorb) on the solid surface are crucial for the fabrication of a stable protein film. Thus, the results described here may facilitate the fabrication of biotechnological and biomedical devices based on protein films.

Declaration of Competing Interest

The authors declare that they have no known competing financial interests or personal relationships that could have appeared to influence the work reported in this paper.

Acknowledgment

This work was partially supported by Grant NCN OPUS2016/23/B/ST5/02788 and Grant NAWA PPN/BIL/2018/1/00103. PK acknowledges the fellowship with the project POWR03.02.0000-I013/16. IB acknowledges support from DAAD project number 57449009. English-language services were provided by stels-ol.de.

Appendix A. Supplementary material

Supplementary data to this article can be found online at https://doi.org/10.1016/j.bioelechem.2021.107946.

References

[1] M.M. Ouberai, K. Xu, M.E. Welland, Effect of the interplay between protein and surface on the properties of adsorbed protein layers, Biomaterials 35 (24) (2014) 6157–6163.
[2] A. Staub, S. Comte, S. Rudaz, J.L. Veuthey, J. Schappler, Use of organic solvent to prevent protein adsorption in CE-MS experiments, Electrophoresis 31 (2010) 3326–3333.
[3] K. Xu, M.M. Ouberai, M.E. Welland, A comprehensive study of lysozyme adsorption using dual polarization interferometry and quartz crystal microbalance with dissipation, Biomaterials 34 (2013) 1461–1470.
[4] O. Santos, T. Nylander, M. Paulsson, C. Trägårdh, Whey protein adsorption onto steel surfaces - effect of temperature, flow rate, residence time and aggregation, J. Food Eng. 74 (2006) 468–483.
[5] M.A. Brusatori, Y. Tie, P.R. Van Tassel, Protein adsorption kinetics under an applied electric field: An optical waveguide lightmode spectroscopy study, Langmuir 19 (2003) 5089–5097.
[6] M. Rabe, D. Verdes, S. Seeger, Understanding protein adsorption phenomena at solid surfaces, Adv. Colloid Interface Sci. 162 (2011) 87–106.
[7] T. Wei, M.A. Carignano, I. Szleifer, Molecular dynamics simulation of lysozyme adsorption/desorption on hydrophobic surfaces, J. Phys. Chem. B 116 (2012) 10189–10194.
[8] D. Stigter, K.A. Dill, Charge effects on folded and unfolded proteins, Biochemistry 29 (5) (1990) 1262–1271.
[9] E. Ficici, D. Jeong, I. Andricioaei, Electric-field-induced protein translocation via a conformational transition in SecDF: an MD study, Biophys. J. 112 (2017) 2520–2528.
[10] Y. Xie, W. Gong, J. Jin, Z. Zhao, Z. Li, J. Zhou, Molecular simulations of lysozyme adsorption on an electrically responsive mixed self-assembled monolayer, Appl. Surf. Sci. 506 (2020) 144962, https://doi.org/10.1016/j.apsusc.2019.144962.
[11] S. Yang, J. Liu, X. Quan, J. Zhou, Bilirubin oxidase adsorption onto charged self-assembled monolayers: insights from multiscale simulations, Langmuir 34 (33) (2018) 9818–9828.
[12] J. Liu, Y. Xie, C. Peng, G. Yu, J. Zhou, Molecular understanding of laccase adsorption on charged self-assembled monolayers, J. Phys. Chem. B 121 (47) (2017) 10610–10617.
[13] L. Rivas, C.M. Soares, A.M. Baptista, J. Simaan, R.E. Di Paolo, D.H. Murgida, P. Hildebrandt, Electric-field-induced redox potential shifts of tetraheme cytochromes c3 immobilized on self-assembled monolayers: surface-enhanced resonance Raman spectroscopy and simulation studies, Biophys. J. 88 (2005) 4188–4199.
[14] V. Lioubimov, A. Kolomenskii, A. Mershin, D.V. Nanopoulos, H.A. Schuessler, Effect of varying electric potential on surface-plasmon resonance sensing, Appl. Opt. 43 (2004) 3426–3432.
[15] R. Morrow, D.R. McKenzie, M.M.M. Bilek, C.L. MacDonald, M. Stindt, G. Anetsberger, A.S. Martin, Electric field effects on adsorption/desorption of proteins and colloidal particles on a gold film observed using surface plasmon resonance, Phys. B Condens. Matter 394 (2007) 203–207.
[16] Z. Jiang, L.e. You, W. Dou, T. Sun, P. Xu, Effects of an electric field on the conformational transition of the protein: a molecular dynamics simulation study, Polymers 11 (2) (2019) 282, https://doi.org/10.3390/polym11020282.
[17] S.R. Tzeng, C.G. Kalodimos, Protein activity regulation by conformational entropy, Nature 488 (2012) 236–240.
[18] J.J. Song, S.K. Smith, G.J. Hannon, L. Joshua-Tor, Crystal structure of Argonaute and its implications for RISC slicer activity, Science 305 (2004) 1434–1437.
[19] A. Dong, J.D. Meyer, B.S. Kendrick, M.C. Manning, J.F. Carpenter, Hydrophobic ion pairing as a method for enhancing structure and activity of lyophilized subtilisin BPN′ suspended in isooctane, Arch. Biochem. Biophys. 334 (1996) 406–414.

[20] J.S. Lee, T. Satoh, H. Shinoda, T. Samejima, S.H. Wu, S.H. Chiou, Effect of heat-induced structural perturbation of secondary and tertiary structures on the chaperone activity of α-crystallin, Biochem. Biophys. Res. Commun. 237 (1997) 277–282.
[21] R. Liang, S. Cheng, X. Wang, Secondary structure changes induced by pulsed electric field affect antioxidant activity of pentapeptides from pine nut (Pinus koraiensis) protein, Food Chem. 254 (2018) 170–184.
[22] I. Bekard, D.E. Dunstan, Electric field induced changes in protein conformation, Soft Matter 10 (3) (2014) 431–437.
[23] H. Olzscha, O. Fedorov, B.M. Kessler, S. Knapp, N.B. La Thangue, CBP/p300 bromodomains regulate amyloid-like protein aggregation upon aberrant lysine acetylation, Cell Chem. Biol. 24 (2017) 9–23.
[24] G.B. Irvine, O.M. El-Agnaf, G.M. Shankar, D.M. Walsh, Protein aggregation in the brain: the molecular basis for Alzheimer's and Parkinson's diseases, Mol. Med. 14 (2008) 451–464.
[25] R.M. Giráldez-pérez, M. Antolín-vallespín, M.D. Muñoz, A. Sánchez-capelo, Models of α-synuclein aggregation in Parkinson's disease, Acta Neuropathol. Commun. (2014) 1–17.
[26] M. Inayathullah, J. Rajadas, Effect of osmolytes on the conformation and aggregation of some amyloid peptides: CD spectroscopic data, Data Br. 7 (2016) 1643–1651.
[27] R.R. Kopito, D. Ron, Conformational disease, Nat. Cell Biol. 2 (11) (2000) E207–E209.
[28] P. Ojeda-May, M.E. Garcia, Electric field-driven disruption of a native β-sheet protein conformation and generation of a helix-structure, Biophys. J. 99 (2010) 595–599.
[29] S.A. Hassan, E.L. Mehler, D. Zhang, H. Weinstein, Molecular dynamics simulations of peptides and proteins with an implicit solvent model based on screened coulomb potentials, Proteins Struct. Funct. Genet. 51 (2003) 109–125.
[30] P. Marracino, M. Casciola, M. Liberti, F. Apollonio, in: Computational Electrostatics for Biological Applications, Springer, Cham, Switzerland, 2015, pp. 255–270.
[31] S. Dongmo, G. Wittstock, J. Christoffers, I. Brand, In situ determination of potential-driven structural changes in a redox-active plumbagin polymer film on a glassy carbon electrode using PM IRRAS under electrochemical control, Electrochim. Acta 255 (2017) 298–308.
[32] M. Tagliazucchi, L.P.M. De Leo, A. Cadranel, L.M. Baraldo, E. Völker, C. Bonazzola, E.J. Calvo, V. Zamlynny, PM IRRAS spectroelectrochemistry of layer-by-layer self-assembled polyelectrolyte multilayers, J. Electroanal. Chem. 649 (2010) 110–118.
[33] M. Ahlers, N. Stein, L. Broch, I.J. Brand, Study of the potential driven changes in a collagen film self-assembled on a polycrystalline gold electrode surface, Electroanal. Chem. 706 (2013) 140–148.
[34] L. Kékedy-Nagy, E.E. Ferapontova, I. Brand, Submolecular structure and orientation of oligonucleotide duplexes tethered to gold electrodes probed by infrared reflection absorption spectroscopy: effect of the electrode potentials, J. Phys. Chem. B 121 (2017) 1552–1565.
[35] R.N. Rambaran, L.C. Serpell, Amyloid fibrils, Prion 2 (3) (2008) 112–117.
[36] S.S.S. Wang, Y.T. Hung, P. Wang, J.W. Wu, The formation of amyloid fibril-like hen egg-white lysozyme species induced by temperature and urea concentration-dependent denaturation Korean, J. Chem. Eng. 24 (2007) 787–795.
[37] J. Wawer, M. Szociński, M. Olszewski, R. Piątek, M. Naczk, J. Krakowiak, Influence of the ionic strength on the amyloid fibrillogenesis of hen egg white lysozyme, Int. J. Biol. Macromol. 121 (2019) 63–70.
[38] F.G.K. Baucke, Further Insight into the Dissociation Mechanism of Glass Electrodes. The Response in Heavy Water, J. Phys. Chem. B 102 (24) (1998) 4835–4841.
[39] B. Jachimska, A. Kozłowska, A. Pajor-Świerzy, Protonation of lysozymes and its consequences for the adsorption onto a mica surface, Langmuir 28 (2012) 11502–11510.
[40] P.J. Artymiuk, C.C.F. Blake, Refinement of human lysozyme at 1.5 A resolution analysis of non-bonded and hydrogen-bond interactions, J. Mol. Biol. 152 (1981) 737–762.
[41] K. Kubiak-Ossowska, M. Cwieka, A. Kaczynska, B. Jachimska, P.A. Mulheran, Lysozyme adsorption at a silica surface using simulation and experiment: effects of pH on protein layer structure, Phys. Chem. Chem. Phys. 17 (2015) 24070–24077.
[42] B. Gilquin, C. Guilbert, D. Perahia, Unfolding of hen egg lysozyme by molecular dynamics simulations at 300K: Insight into the role of the interdomain interface, Proteins Struct. Funct. Genet. 41 (2000) 58–74.
[43] N.J. Greenfield, G.D. Fasman, Computed circular dichroism spectra for the evaluation of protein conformation, Biochemistry 8 (10) (1969) 4108–4116.
[44] G. Holzwarth, P. Doty, The ultraviolet circular dichroism of polypeptides, J. Am. Chem. Soc. 87 (1965) 218–228.
[45] R.N. Rambaran, L.C. Serpell, Amyloid fibrils. Abnormal protein assembly, Prion 2 (3) (2008) 112–117.
[46] T. Wei, M.A. Carignano, I. Szleifer, Lysozyme adsorption on polyethylene surfaces: why are long simulations needed, Langmuir 27 (2011) 12074–12081.
[47] P. Komorek, M. Wałek, B. Jachimska, Mechanism of lysozyme adsorption onto gold surface determined by quartz crystal microbalance and surface plasmon resonance, Bioelectrochemistry 135 (2020) 107582, https://doi.org/10.1016/j.bioelechem.2020.107582.
[48] J. Clavilie, N.J. Vanhuong, Study on structure of double film on gold electrodes, Electroanal. Chem. 41 (1973) 193–199.
[49] O.J. Murphy, J.S. Wainright, Spectroscopic investigations of porous and sealed anodic alumina films, Proc. - Electrochem. Soc. 86–7 (1986) 483–497.
[50] S.A. Tatulian, in: Lipid-Protein Interactions. Methods in Molecular Biology (Methods and Protocols), Humana Press, Totowa, NJ, 2013, pp. 177–218.
[51] A. Miranker, S.E. Radford, M. Karplus, C.M. Dobson, Demonstration by NMR of folding domains in lysozyme, Nature 349 (1991) 633–636.
[52] B.A. Russell, B. Jachimska, P. Komorek, P.A. Mulheran, Y. Chen, Lysozyme encapsulated gold nanoclusters: effects of cluster synthesis on natural protein characteristics, Phys. Chem. Chem. Phys. 19 (2017) 7228–7235.
[53] L.G. Astrakas, C. Gousias, M. Tzaphlidou, Electric field effects on alanine tripeptide in sodium halide solutions, Electromagn. Biol. Med. 34 (4) (2015) 361–369.
[54] D.T. Kim, H.W. Blanch, C.J. Radke, Direct imaging of lysozyme adsorption onto mica by atomic force microscopy, Langmuir 18 (2002) 5841–5850.
[55] H. Lei, M. Wang, Z. Tang, Y. Luan, W. Liu, B. Song, H. Chen, Control of lysozyme adsorption by pH on surfaces modified with polyampholyte brushes, Langmuir 30 (2014) 501–508.
[56] M. van der Veen, W. Norde, M.C. Stuart, Electrostatic interactions in protein adsorption probed by comparing lysozyme and succinylated lysozyme, Colloids Surf. B Biointerfaces 35 (1) (2004) 33–40.
[57] T. Nezu, T. Masuyama, K. Sasaki, S. Saitoh, M. Taira, Y. Araki, Effect of pH and addition of salt on the adsorption behavior of lysozyme on gold, silica, and titania surfaces observed by quartz crystal microbalance with dissipation monitoring, Dent. Mater. J. 27 (2008) 573–580.
[58] G. Yu, J. Liu, J. Zhou, Mesoscopic coarse-grained simulations of lysozyme adsorption, J. Phys. Chem. B 118 (2014) 4451–4460.
[59] S.G. Booth, B. Felisilda, E. Alvarez De Eulate, O.J.R. Gustafsson, M. Arooj, R.L. Mancera, R.A.W. Dryfe, M.J. Hackett, S.G. Booth, Molecular dynamics simulation of biophysical phenomena, Langmuir 35 (2019) 5821–5829.
[60] B. Czarnik-Matusewicz, K. Murayama, Y. Wu, Y.J. Ozaki, Two-dimensional infrared, two-dimensional Raman, and two-dimensional infrared and Raman heterospectral correlation studies of secondary structure of β-Lactoglobulin in buffer solutions, Phys. Chem. B 104–32 (2000) 7803–7811.
[61] T.J. Kamerzell, C.R. Middaugh, Two-dimensional correlation spectroscopy reveals coupled immunoglobulin regions of differential flexibility that influence stability, Biochemistry 46 (2007) 9762–9773.
[62] A. Barth, Infrared spectroscopy of proteins, Biochim. Biophys. Acta - Bioenerg. 1767 (2007) 1073–1101.
[63] W.K. Surewicz, H.H. Mantsch, D. Chapman, Determination of protein secondary structure by Fourier transform infrared spectroscopy: a critical assessment, Biochemistry 32 (1993) 389–394.
[64] R. Armen, D.O.V. Alonso, V. Daggett, The role of α-, 3_{10}-, and π-helix in helix→coil transitions, Protein Sci. 12 (2003) 1145–1157.
[65] V. Serrano, W. Liu, S. Franzen, An infrared spectroscopic study of the conformational transition of elastin-like polypeptides, Biophys. J. 93 (2007) 2429–2435.
[66] V. Militello, C. Casarino, A. Emanuele, A. Giostra, F. Pullara, M. Leone, Aggregation kinetics of bovine serum albumin studied by FTIR spectroscopy and light scattering, Biophys. Chem. 107 (2004) 175–187.
[67] J. Zurdo, J.I. Guijarro, J.L. Jiménez, H.R. Saibil, C.M. Dobson, Folding versus aggregation: polypeptide conformations on competing pathways, J. Mol. Biol. 311 (2001) 325–340.
[68] F. Ruggeri, F. Zhang, T. Lind, E.D. Bruce, B.L.T. Lau, M. Cárdenas, Non-specific interactions between soluble proteins and lipids induce irreversible changes in the properties of lipid bilayers, Soft Matter 9 (2013) 4219–4226.
[69] R. Sarroukh, E. Goormaghtigh, J.M. Ruysschaert, V. Raussens, ATR-FTIR: a "rejuvenated" tool to investigate amyloid proteins, Biochim. Biophys. Acta - Biomembr. 1828 (2013) 2328–2338.
[70] C.T. Chang, C.S.C. Wu, J.T. Yang, Circular dichroic analysis of protein conformation: inclusion of the β-turns, Anal. Biochem. 91 (1978) 13–31.
[71] T. Knubovets, J.J. Osterhout, A.M. Klibanov, Structure of lysozyme dissolved in neat organic solvents as assessed by NMR and CD spectroscopies, Biotechnol. Bioeng. 63 (1999) 242–248.
[72] T. Knubovets, J.J. Osterhout, P.J. Connolly, A.M. Klibanov, Structure, thermostability, and conformational flexibility of hen egg-white lysozyme dissolved in glycerol, Proc. Natl. Acad. Sci. USA 96 (1999) 1262–1267.
[73] X. Wu, G. Narsimhan, Effect of surface concentration on secondary and tertiary conformational changes of lysozyme adsorbed on silica nanoparticles, Biochim. Biophys. Acta - Proteins Proteomics 1784 (11) (2008) 1694–1701.
[74] T.F. Kumosinski, H.M. Farrell, Determination of the global secondary structure of proteins by Fourier transform infrared (FTIR) spectroscopy, Trends Food Sci. Technol. 4 (1993) 169–175.
[75] D. Frishman, P. Argos, Knowledge-based protein secondary structure assignment, Proteins Struct. Funct. Bioinforma. 23 (1995) 566–579.
[76] A.R. Rees, R.E. Offord, X-ray crystallography and the amino acid sequence of lysozyme, Biochem. J. 130 (1972) 965–968.
[77] T.D. Murray, A.Y. Lyubimov, C.M. Ogata, H. Vo, M. Uervirojnangkoorn, A.T. Brunger, J.M. Berger, A high-transparency, micro-patternable chip for X-ray diffraction analysis of microcrystals under native growth conditions, Acta Crystallogr. Sect. D Biol. Crystallogr. 71 (2015) 1987–1997.
[78] C. Redfield, C.M. Dobson, Proton NMR studies of human lysozyme: spectral assignment and comparison with hen lysozyme, Biochemistry 29 (31) (1990) 7201–7214.
[79] V.K. Laurinavichyute, S. Nizamov, V.M. Mirsky, The role of anion adsorption in the effect of electrode potential on surface plasmon resonance response, ChemPhysChem 18 (2017) 1552–1560.

[80] M. Kasuya, T. Sogawa, T. Masuda, T. Kamijo, K. Uosaki, K. Kurihara, Anion adsorption on gold electrodes studied by electrochemical surface forces measurement, J. Phys. Chem. C 120 (2016) 15986–15992.
[81] J. Israelachvili (Ed.), Intermolecular and surface forces, third ed., Open Library, London, United Kingdom, 1991.
[82] M. Buck, S.E. Radford, C.M. Dobson, A partially folded state of hen egg white lysozyme in trifluoroethanol: structural characterization and implications for protein folding, Biochemistry 32 (1993) 669–678.
[83] S. Bhattacharjya, P. Balaram, Effects of organic solvents on protein structures: Observation of a structured helical core in hen egg-white lysozyme in aqueous dimethylsulfoxide, Proteins Struct. Funct. Genet. 29 (1997) 492–507.